Supplementary Data

Reverse genetics-based biochemical studies of the ribosomal exit tunnel constriction region in eukaryotic ribosome stalling: Spatial allocation of the regulatory nascent peptide at the constriction

Seidai Takamatsu[1], Yubun Ohashi[2], Noriyuki Onoue[1], Yoko Tajima[3], Tomoya Imamichi[1], Shinya Yonezawa[1], Kyoko Morimoto[3], Hitoshi Onouchi[2,3,4], Yui Yamashita[2,3,4,*] and Satoshi Naito[1,3,4,*]

[1]Division of Life Science, Graduate School of Life Science, Hokkaido University, Sapporo 060-0810, Japan

[2]Frontiers in Biosciences, Graduate School of Agriculture, Hokkaido University, Sapporo 060-8589, Japan

[3]Department of Applied Bioscience, Faculty of Agriculture, Hokkaido University, Sapporo 060-8589, Japan

[4]Research Group of Applied Bioscience, Research Faculty of Agriculture, Hokkaido University, Sapporo 060-8589, Japan

[*]To whom correspondence should be addressed: Satoshi Naito. Tel: +81-11-706-2800; Fax: +81-11-706-4932; Email: naito@abs.agr.hokudai.ac.jp

Correspondence may also be addressed to Yui Yamashita. Tel: +81-11-706-3888; Fax: +81-11-706-4932; Email: yuiyama@abs.agr.hokudai.ac.jp

Contents

Supplementary Results 1.1. – 1.6. ……. 2
Supplementary Figures S1 – S17 ……..……. 5
Supplementary Tables S1 – S2 ……. 22
Supplementary References ……..…….. 25

Supplementary Results

1.1. The CGS1 System in Col-0 ACE.

To determine the effects of mutant uL4D-containing ribosomes on AdoMet-induced NPmRS, we used *GST:CGS1*(*WT*) RNA (Figure 5A and Supplementary Figure S6A). The 183-amino-acid sequence of the *CGS1* exon 1 coding sequence, which contains the MTO1 region, is necessary and sufficient for AdoMet-induced NPmRS (37). The MTO1 region is the *cis* element for the AdoMet-induced NPmRS that occurs at Ser-94 (21).

AdoMet-induced NPmRS of CGS1 has been extensively studied by using WGE (17–22), but is only partially characterized in ACE (23). At the standard RNA concentration used in ACE (50 fmol μl^{-1}), a second ribosome is stacked behind the initially stalled ribosome (19), and two peptidyl-tRNA species, PtR-I and PtR-II, are produced in ACE *in vitro* translation (Supplementary Figure S6B). To determine which one of the peptidyl-tRNA bands corresponds to the initially stalled ribosome at Ser-94, increasing amounts of *GST:CGS1*(*WT*) RNA were translated in Col-0 ACE (Supplementary Figure S6C and D). By increasing the amount of RNA to be translated, the relative intensity of the peptidyl-tRNA that corresponds to the secondary stalled ribosome will be reduced (19), because the number of ribosomes on one mRNA is reduced. The result indicated that PtR-I is the initially stalled ribosome at Ser-94, while PtR-II is the secondarily stalled ribosome. To confirm this, we analyzed the puromycin sensitivity of the peptidyl-tRNA (Supplementary Figure S6E and F). We previously reported that the initially stalled ribosome at Ser-94 exhibits lower reactivity to puromycin than the secondarily stalled ribosome in WGE (19). The results also indicated that PtR-I corresponds to the initially stalled ribosome at Ser-94. Therefore, PtR-I band intensities were measured in Figure 5A.

mto1-1 mutation (G84S) abolishes AdoMet-induced NPmRS of CGS1 (17,21,22). Translation of *GST:CGS1*(*mto1-1*) RNA (Supplementary Figure S6A) in Col-0 ACE in the presence of AdoMet did not show peptidyl-tRNA accumulation (Supplementary Figure S6B). These results show that the AdoMet-induced NPmRS of CGS1 is recapitulated in Col-0 ACE (23).

1.2. The hCMV System in Col-0 ACE

The 22-amino-acid nascent peptide of hCMV *gp48* uORF2 causes ribosome stalling autonomously to downregulate *gp48* expression during the early stages of infection (28,65). This reaction occurs in WGE and the structure of stalled ribosome in WGE has been solved by cryo-EM (14,16), but has not been studied in ACE.

Autonomous ribosome stalling of the hCMV system was analyzed in Col-0 ACE (Supplementary Figure S10). *TagI:DP75:hCMV* RNA (Supplementary Figure S10B) carries *M8:His:HA* tags (*TagI*) and DP75 linker fused in-frame to the N-terminus of hCMV *gp48* uORF2. DP75 linker (15,43) was used to facilitate the detection of short polypeptide. After the translation of *TagI:DP75:hCMV*(*WT*) RNA in Col-0 ACE, translation products were analyzed by immunoblotting using anti-HA antibody, which detected 15-kDa full-length product and RNase-sensitive 37-kDa peptidyl-tRNA bands. In contrast, the translation of *TagI:DP75:hCMV*(*P21A*) RNA produced only 15-kDa full-length product (Supplementary Figure S10C). The *P21A* mutation has been reported to abolish the NPmRS (15,28). The results show that autonomous ribosome stalling of the hCMV system is recapitulated in Col-0 ACE.

For the reporter assay in Figure 7A, *5′-hCMV:LUC* RNA that carries the 5′-UTR of hCMV *gp48* fused to *LUC* reporter gene (Supplementary Figure S10D) was used.

1.3. The AAP System in Col-0 ACE

N. crassa arg-2 codes for an enzyme involved in L-arginine biosynthesis. The 24-amino-acid nascent peptide of AAP, the sequence encoded by *arg-2* uORF, directs the ribosome to stall in response to L-arginine during translation termination of AAP in WGE (24,25). This reaction occurs in WGE and the structure of the stalled ribosome in WGE has been solved by cryo-EM (14), but has not been analyzed in ACE.

L-Arginine-induced ribosome stalling of the AAP system was analyzed in Col-0 ACE (Supplementary Figure S12). Since anti-HA antibody only poorly detected the translation products, the

experiments were carried out using *TagII:DP75:AAP* RNA that carry *M8:His:HA:3xFLAG:Myc* tag sequences (Supplementary Figure S12B) and the translation products were detected using anti-FLAG antibody. Translation of *TagII:DP75:AAP*(*WT*) RNA in the presence of 2.08 mM L-arginine produced RNase-sensitive 40-kDa peptidyl-tRNA in addition to 25-kDa full-length product, and the peptidyl-tRNA accumulation was evidently detected at 10 min after the start of translation (Supplementary Figure S12C). The accumulation of 40-kDa peptidyl-tRNA was also detected with 0.08 mM L-arginine, which is the basal L-arginine concentration in ACE (23), although the level of accumulation was lower than at 2.08 mM. This is consistent with a previous report describing that L-arginine-induced stalling was observed even at 0.01 mM (24). The accumulation of peptidyl-tRNA was diminished when *TagII:DP75:AAP*(*D12N*) RNA was translated in the presence of 2.08 mM L-arginine (Supplementary Figure S12C and D). The *D12N* mutation has been reported to abolish L-arginine-induced NPmRS of AAP (24). The results show that L-arginine-induced NPmRS of AAP is recapitulated in Col-0 ACE.

1.4. The AtAMD1 System in Col-0 ACE

AtAMD1 codes for an enzyme involved in spermidine and spermine biosynthesis in Arabidopsis. The 52-amino-acid nascent peptide of S-uORF directs the ribosome to stall in response to high concentrations of polyamines during translation termination of S-uORF in WGE (31). This reaction is only partially characterized in ACE (31).

Polyamine-induced ribosome stalling of the AtAMD1 system was analyzed in Col-0 ACE (Supplementary Figure S13). As an effector, spermidine was used in the present study (31). Polyamines are necessary for *in vitro* translation, but are inhibitory at high concentrations. We previously determined spermidine concentrations for stalling assays of AtAMD1 in WGE (31). In the present study, we confirmed that the same concentrations of spermidine (0.2 mM and 0.7 mM as control and stalling conditions, respectively) can be used in ACE. The spermidine concentration for the standard translation reaction in ACE is 0.5 mM (23).

TagI:DP75:S-uORF(*WT*) RNA (Supplementary Figure S13B) was translated in Col-0 ACE in the presence of 0.2 or 0.7 mM spermidine and analyzed by immunoblotting using anti-HA antibody (Supplementary Figure S13C). In the presence of 0.7 mM spermidine, RNase-sensitive 37-kDa peptidyl-tRNA was detected in addition to 18-kDa full-length product, and the accumulation of peptidyl-tRNA was dependent on the spermidine concentration (Supplementary Figure S13D and E). Introduction of a frame-shift mutation in S-uORF abolished the peptidyl-tRNA accumulation (Supplementary Figure S13C), as previously reported (31). These results show that polyamine-induced NPmRS of AtAMD1 is recapitulated in Col-0 ACE.

For the reporter assay in Figure 7B, *5′-AtAMD1:LUC* RNA that carries the 5′-UTR of *AtAMD1* (Supplementary Figure S13A) fused to *LUC* reporter gene (Supplementary Figure S13F) was used. When the RNA carrying the WT S-uORF sequence was translated in Col-0 ACE, the reporter activity was reduced as the concentration of spermidine was increased, whereas the reporter activity was significantly higher if the S-uORF sequence bears a frame-shift mutation (Supplementary Figure S13G).

1.5. The MAGDIS System in Col-0 ACE

mAMD1 codes for an enzyme involved in spermidine and spermine biosynthesis in mammals. The six-amino-acid uORF sequence, MAGDIS, of *mAMD1* directs the ribosome to stall in response to high concentrations of polyamines in WGE (32,33). The ribosome stalling occurs at the termination codon of the uORF (32,33). Both *mAMD1* and *AtAMD1* genes codes for AdoMet decarboxylase, and are regulated by a uORF in a polyamine-dependent manner. However, the lengths and amino acid sequences of the uORFs are quite different.

Polyamine-induced ribosome stalling of the MAGDIS system was analyzed in Col-0 ACE (Supplementary Figure S14). Since anti-HA antibody barely detected a peptidyl-tRNA band, *TagII:DP75:MAGDIS*(*WT*) RNA (Supplementary Figure S14B) was translated in Col-0 ACE in the presence of 0.2 or 0.7 mM spermidine. Immunoblot analysis using anti-FLAG antibody detected double bands of ~38-kDa peptidyl-tRNA when translated in the presence of 0.7 mM spermidine, while 20-kDa full-length product predominated when translated in 0.2 mM spermidine (Supplementary Figure S14C,

lanes 1 and 2). The accumulation of peptidyl-tRNA was evident at 10 min of translation (Supplementary Figure S14D) and was dependent on the spermidine concentration (Supplementary Figure S14E and F). When *TagII:DP75:MAGDIS*(*I5L*) RNA, which carries a mutation that abolishes the polyamine-dependent NPmRS of MAGDIS (32), was used, peptidyl-tRNA accumulation was diminished. These results show that polyamine-induced NPmRS of *mAMD1* is recapitulated in Col-0 ACE. Although the origin of the double bands for the peptidyl-tRNA is unknown, the intensities of the two bands paralleled in each of the experiments in Supplementary Figure S14. Therefore, we used both bands for calculation of stalling efficiencies in Supplementary Figure S14F and Figure 5E.

For the reporter assay in Figure 7C, *5′-mAMD1:LUC* RNA that carries the 5′-UTR of *mAMD1* (Supplementary Figure S14A) fused to *LUC* reporter gene (Supplementary Figure S14G) was used.

1.6. The AUG-Stop System in Col-0 ACE

The expression of Arabidopsis *NIP5;1*, encoding a boric acid transporter, is downregulated by ribosome stalling in response to high concentrations of boric acid at the minimum uORF, AUG-Stop, which is coupled with *NIP5;1* mRNA degradation in WGE. We used a 306-nt 5'-UTR containing uORF3 and uORF4 (Supplementary Figure S17A and B) (34), of which uORF4 is the AUG-Stop. In general, at both the start and the termination codons, decoding by the ribosome takes longer than at other codons, and boric acid induces prolonged ribosome stalling at AUG-Stop. For this response, the AUG codon has to be directly followed by one of the stop codons, and insertion of even a single codon is detrimental to the response (34). This reaction has been studied in WGE (34), but not in ACE.

When *5′-NIP5;1*(*WT*)*:LUC* RNA (Supplementary Figure S17B) was translated in Col-0 ACE, relative reporter activity was reduced in a boric acid-dependent manner. In contrast, disruption of AUG abolished the response (Supplementary Figure S17C). These results show that the response of AUG-Stop to boric acid is recapitulated in Col-0 ACE.

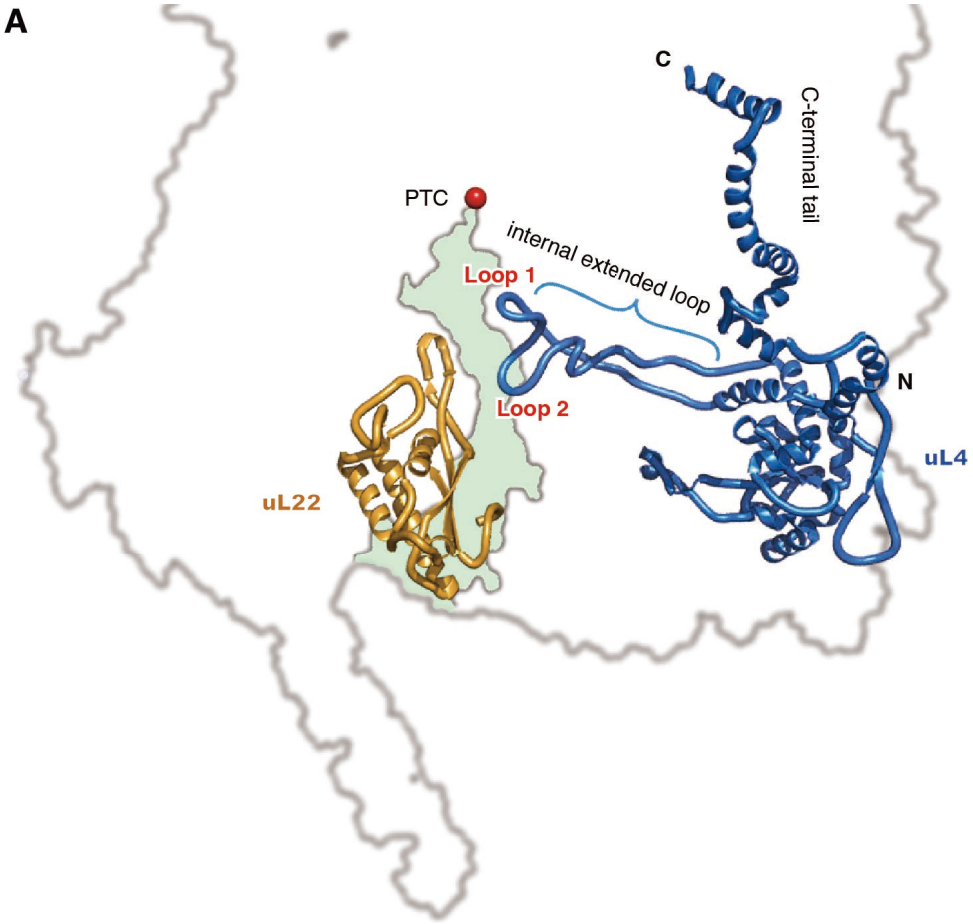

Supplementary Figure S1. Structure and amino acid sequence alignment of uL4. (**A**) Structure of wheat uL4 deduced by cryo-EM (PDB 4V7E) (54). The internal extended loop, Loops 1 and 2, C-terminal tail, and N- and C-termini of uL4 are marked. uL22, the exit tunnel (light green), and PTC are also shown.

Next page: (**B**) Alignment of amino acid sequences of Arabidopsis uL4 paralogs, uL4A (At_uL4A; GenBank accession no. NP_187574) and uL4D (At_uL4D; accession no. NP_195907), wheat (*Triticum aestivum*) uL4 (Ta_uL4; Ensembl Plants id TraesCS4A02G091100), and yeast paralogs uL4A (Sc_uL4A; accession no. NP_009587) and uL4B (Sc_uL4B; accession no. NP_010295) were aligned using ClustalW (http://www.ebi.ac.uk/Tools/msa/clustalw2/). Alignments of Arabidopsis paralogs alone (At), and Arabidopsis and wheat alone (At/Ta) are also shown. Identical (asterisks) and similar (dots and colons) amino acid residues are marked. Regions of the internal extended loop (blue line) and β-loops (Loops 1 and 2; red lines) are marked above the Ta_uL4 sequence. Substituted amino acid in *R77A*, deleted amino acids in *ΔTV*, and *Δloop* mutations in At_uL4D are reversed in violet, reversed in magenta, and underlined in brown, respectively. Wheat is hexaploid and has several copies of uL4 in its genome. One of the uL4 paralogs on chromosome 4A is shown here (66).

B

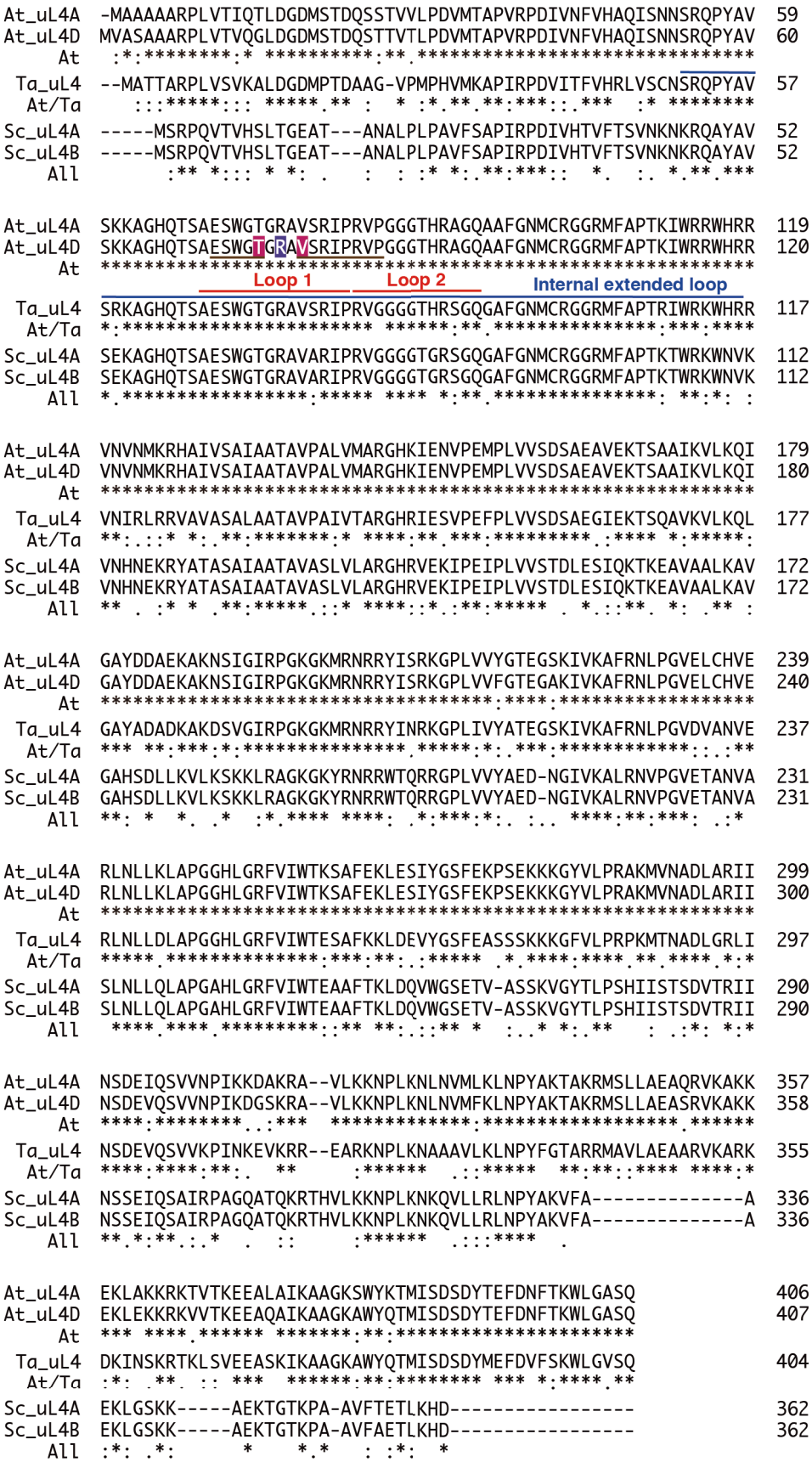

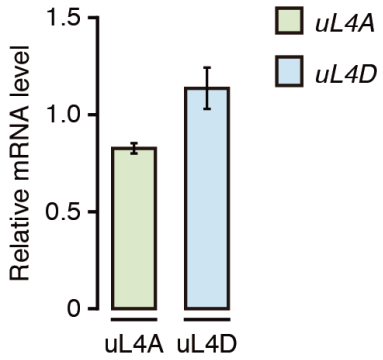

Supplementary Figure S2. Accumulation levels of *uL4A* and *uL4D* mRNAs in wild-type Col-0 plants. Total RNA was extracted from rosette leaves 4 weeks after imbibition. *uL4A* and *uL4D* mRNAs were quantified by qRT-PCR using *UBQ5* mRNA as a control. Relative amounts of *uL4A* and *uL4D* mRNAs were calculated by using known amounts of *uL4A* and *uL4D* cDNAs as standards.

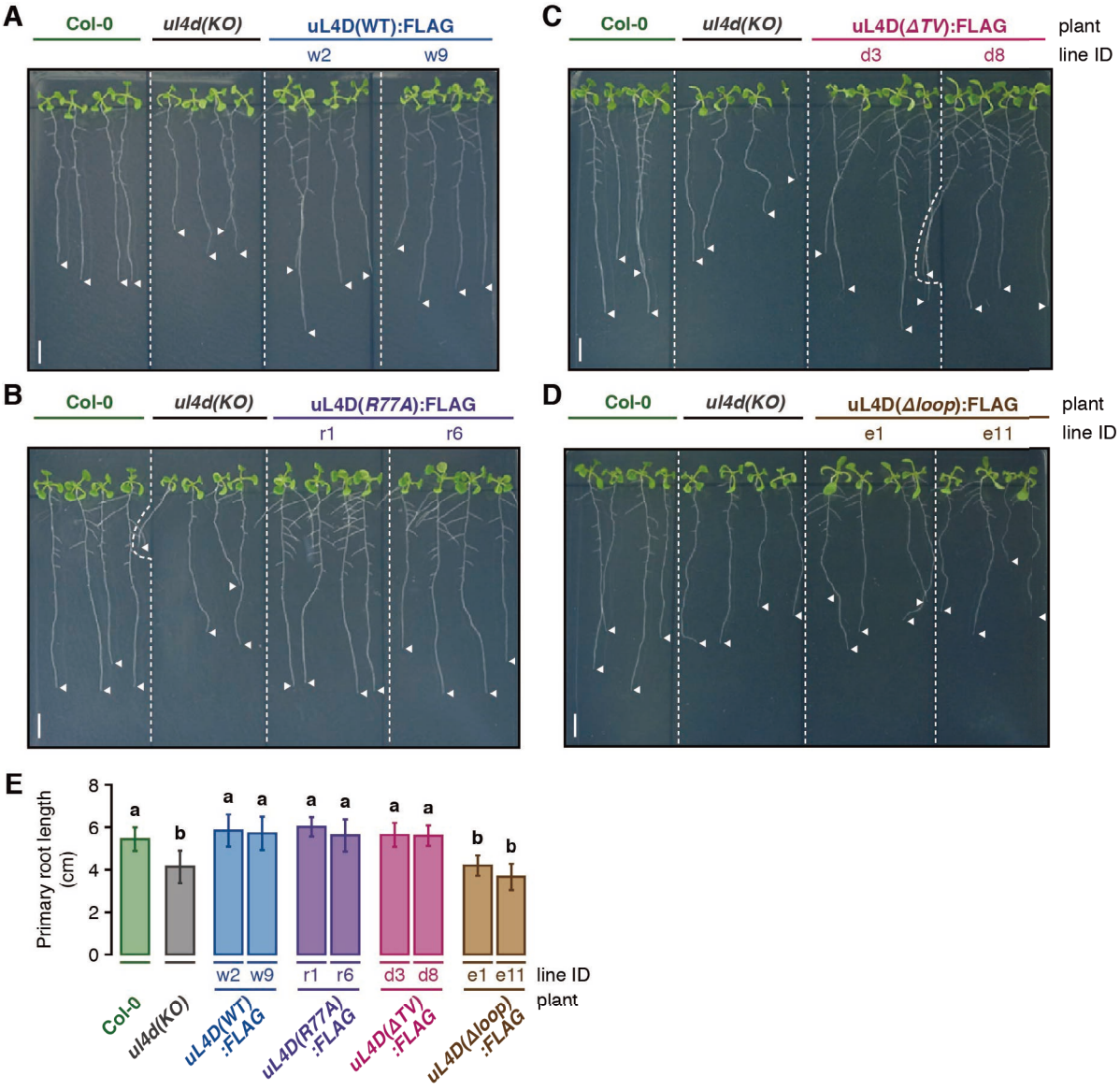

Supplementary Figure S3. FLAG-tagged uL4Ds complement the short-root phenotype of *ul4d(KO)* plants. Wild-type Col-0 plants, *ul4d(KO)*, and transgenic plants expressing FLAG-tagged uL4D(WT) (**A**), uL4D(*R77A*) (**B**), uL4D(*ΔTV*) (**C**), or uL4D(*Δloop*) (**D**) were grown for 10 days on half-strength MS medium plates under long-day conditions. Arrowheads indicate the tip of the primary roots. Bars = 10 mm. (**E**) Primary root lengths in (A–D) were measured and means ± SD ($n > 7$) are shown. Different letters indicate significant differences ($p < 0.05$, Tukey-Kramer test).

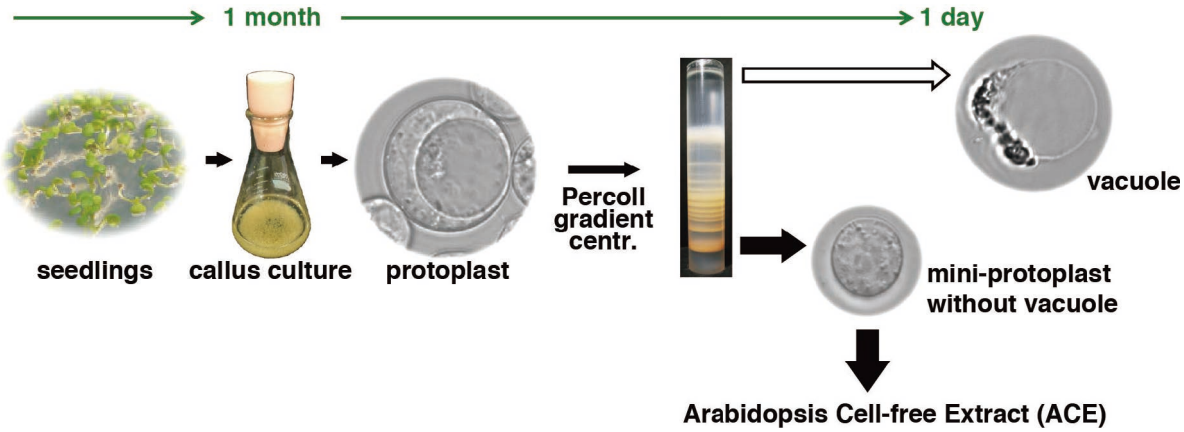

Supplementary Figure S4. Outline of the preparation of ACE *in vitro* translation system from Arabidopsis seedlings (23). One-week-old Arabidopsis seedlings were minced and were cultured with rotatory shaking in the dark. The culture medium was changed every 6 days. Three days after the third medium change, protoplasts were prepared. Plant cells have a large central vacuole that contains nucleases and proteases. The protoplasts were subjected to Percoll gradient centrifugation to obtain evacuolated mini-protoplasts from which vacuoles were removed. The evacuolated mini-protoplasts were disrupted using a Dounce homogenizer and the lysate was used to prepare an ACE *in vitro* translation cocktail. ACE can be prepared 1 month after sowing Arabidopsis seeds. Note that the ACE preparation protocol (23) has a typographical error of m/μ (67).

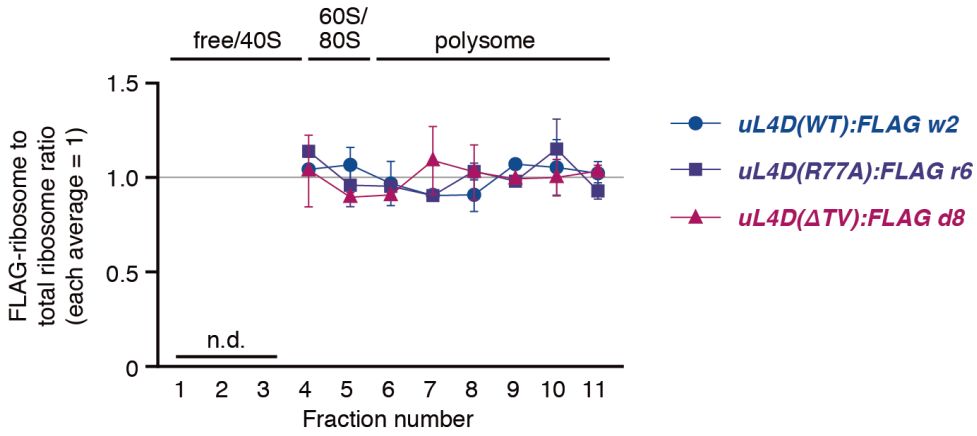

Supplementary Figure S5. Distribution of FLAG-tagged mutant uL4D-containing ribosomes in the polysome profiling. The immunoblot signals in Figure 4B were quantified and the distributions of FLAG-tagged mutant uL4D-containing ribosomes (detected by using anti-FLAG antibody) among total ribosome (detected by using anti-uL22 antiserum) were calculated. The positions of free proteins and 40S subunit, 60S subunit, 80S ribosome, and polysome fractions are indicated. The y-axis was set so that the means of uL4D(WT):FLAG w2 line, uL4D(*R77A*):FLAG r6 line, and uL4D(*ΔTV*):FLAG d8 line are 1. Means ± SD of two biological repeats are shown.

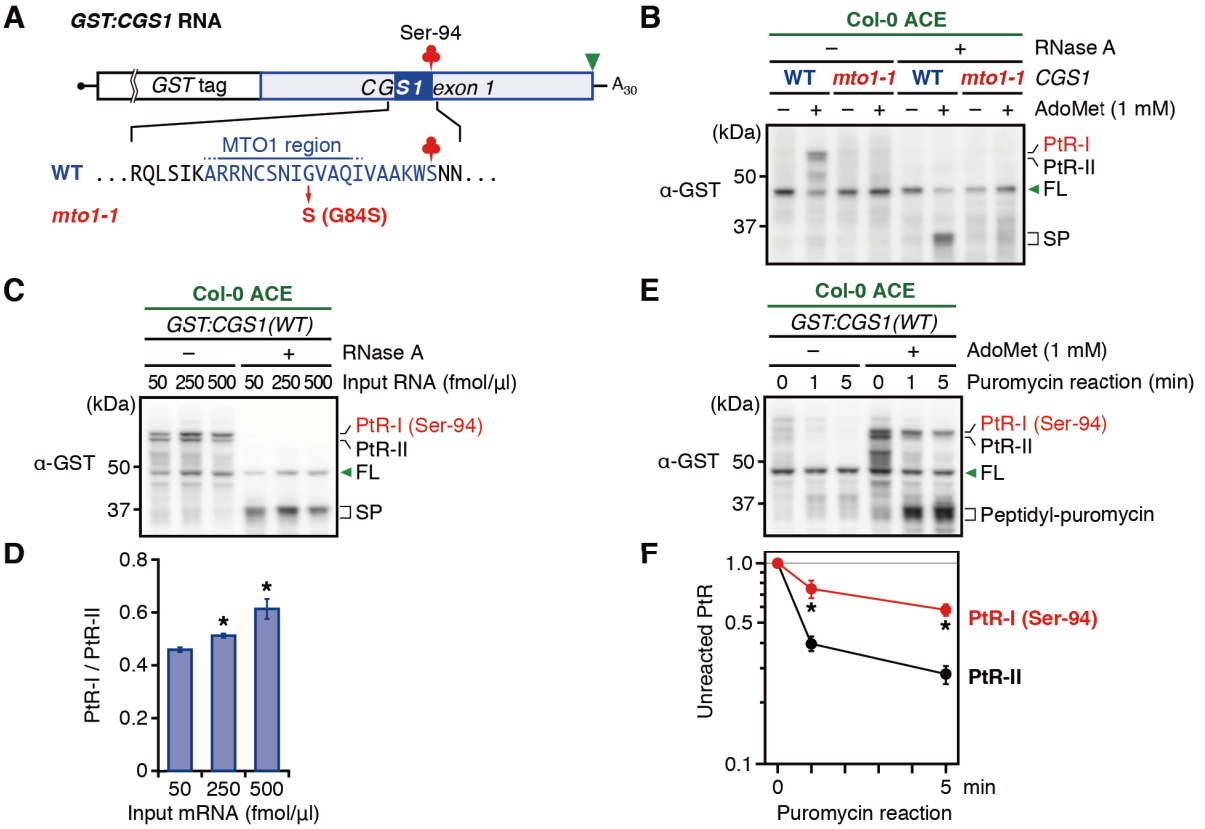

Supplementary Figure S6. The CGS1 system in Col-0 ACE. (**A**) Schematic representation of *GST:CGS1* RNA used for stalling assay (Figure 5A). The RNA carries a glutathione *S*-transferase (GST) tag sequence fused in-frame to the N-terminus of the *CGS1* exon 1 coding sequence (17,68). The amino acid sequences around the MTO1 region of the wild-type (WT) *CGS1* and *mto1-1* (G84S) mutation are shown. AdoMet-induced NPmRS occurs at Ser-94 (red clover). The MTO1 region (21) is indicated. (**B**) *GST:CGS1*(*WT*) and *GST:CGS1*(*mto1-1*) RNAs (50 fmol µl^{-1}) were translated in Col-0 ACE for 30 min in the absence (–) or presence (+) of 1 mM AdoMet. In RNase + lanes, samples were treated with RNase A before separation by SDS-PAGE. The positions of the 45-kDa full-length product (FL), the ~55-kDa peptidyl-tRNAs (PtR-I and PtR-II), and the 35-kDa stalled peptide (SP) produced by RNase A treatment are indicated. A representative result of duplicate experiments is shown. (**C**) *GST:CGS1*(*WT*) RNA was translated in Col-0 ACE at different RNA concentrations for 30 min. In RNase + lanes, samples were treated with RNase A before separation by SDS-PAGE. A representative result of triplicate experiments is shown. Bands are marked as in (B). (**D**) The immunoblot signals in (C) were quantified and relative intensity of PtR-I to PtR-II was calculated. Means ± SD of three independent experiments are shown. Asterisks indicate significant differences compared with the standard condition at 50 fmol µl^{-1} RNA ($p < 0.05$, Welch's *t*-test). (**E**) *GST:CGS1*(*WT*) RNA was translated in Col-0 ACE. After 30 min of translation, puromycin was added at a final concentration of 2 mM and samples were withdrawn at the indicated time points. The position of the 35-kDa peptidyl-puromycin is indicated. A representative result of triplicate experiments is shown. (**F**) The immunoblot signals in (E) were quantified, and the intensity of unreacted peptidyl-tRNA was normalized to that at time 0. Means ± SD of three independent experiments are shown. Asterisks indicate significant differences between PtR-I and PtR-II at each time point ($p < 0.05$, Welch's *t*-test).

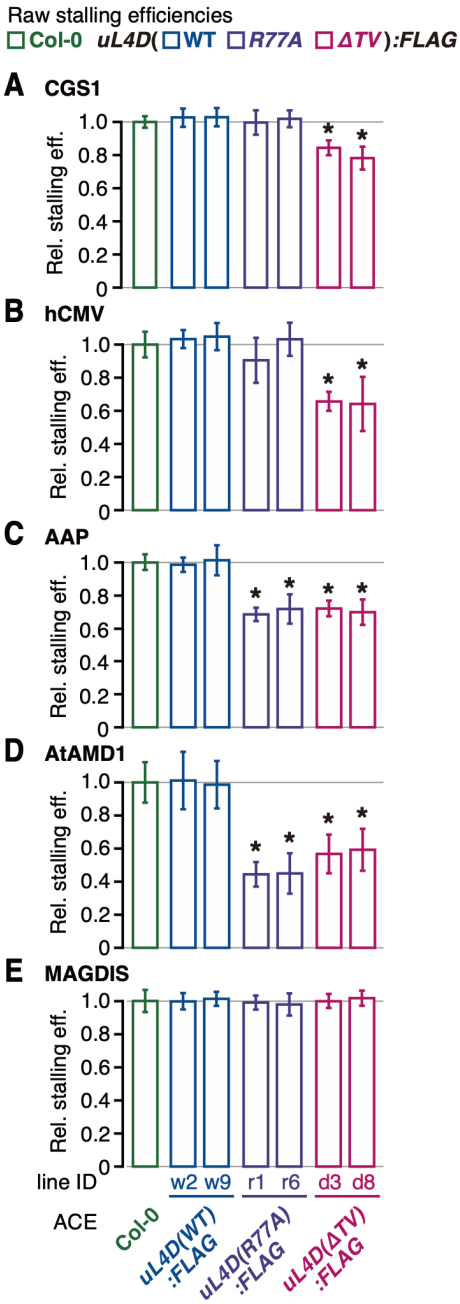

Supplementary Figure S7. Raw stalling efficiencies. (**A**–**E**) The raw stalling efficiencies corresponding to the right panels of Figure 5A–E, respectively, are shown. Asterisks indicate significant differences compared with Col-0 ACE ($q < 0.05$ by Welch's *t*-test with FDR correction).

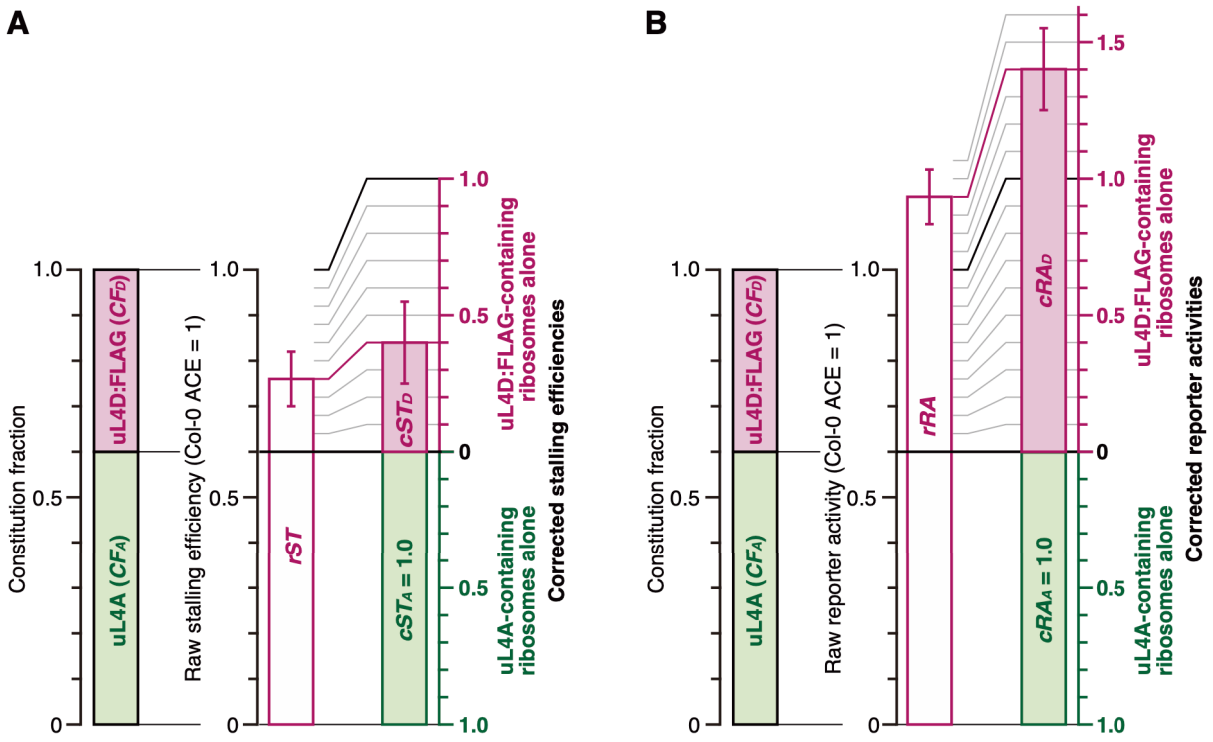

Supplementary Figure S8. Correction of raw values of stalling efficiencies and reporter activities for the constitution fraction of uL4D mutant ribosome.

(**A**) Correction of the stalling efficiency. The raw stalling efficiency relative to Col-0 ACE (*rST*) contains contributions from both FLAG-tagged mutant uL4D- and endogenous uL4A-containing ribosomes. To evaluate the stalling efficiencies of the mutant uL4D-containing ribosomes alone, we calculated the corrected stalling efficiencies (cST_D) by taking the constitution fraction of mutant uL4D-containing ribosomes (CF_D):

$rST = CF_A + CF_D \times cST_D$, where $CF_A = 1 - CF_D$.

Therefore,

$cST_D = 1 - (1 - rST) / CF_D$.

SD values before (*rSD*) and after correction (cSD_D) are,

$cSD_D = rSD / CF_D$.

This calculation assumes that the stalling efficiency of endogenous uL4A-containing ribosomes alone (cST_A) is the same as that in Col-0 ACE (*i.e.*, $cST_A = 1$), which we believe is reasonable. The *rSD* value is ascribed all to cSD_D in this calculation.

(**B**) Correction of the reporter activity. Likewise, the raw reporter activity relative to Col-0 ACE (*rRA*) and its SD values (*rSD*) were corrected for the constitution fraction of mutant uL4D-containing ribosomes (CF_D):

$cRA_D = 1 - (1 - rRA) / CF_D$

$cSD_D = rSD / CF_D$.

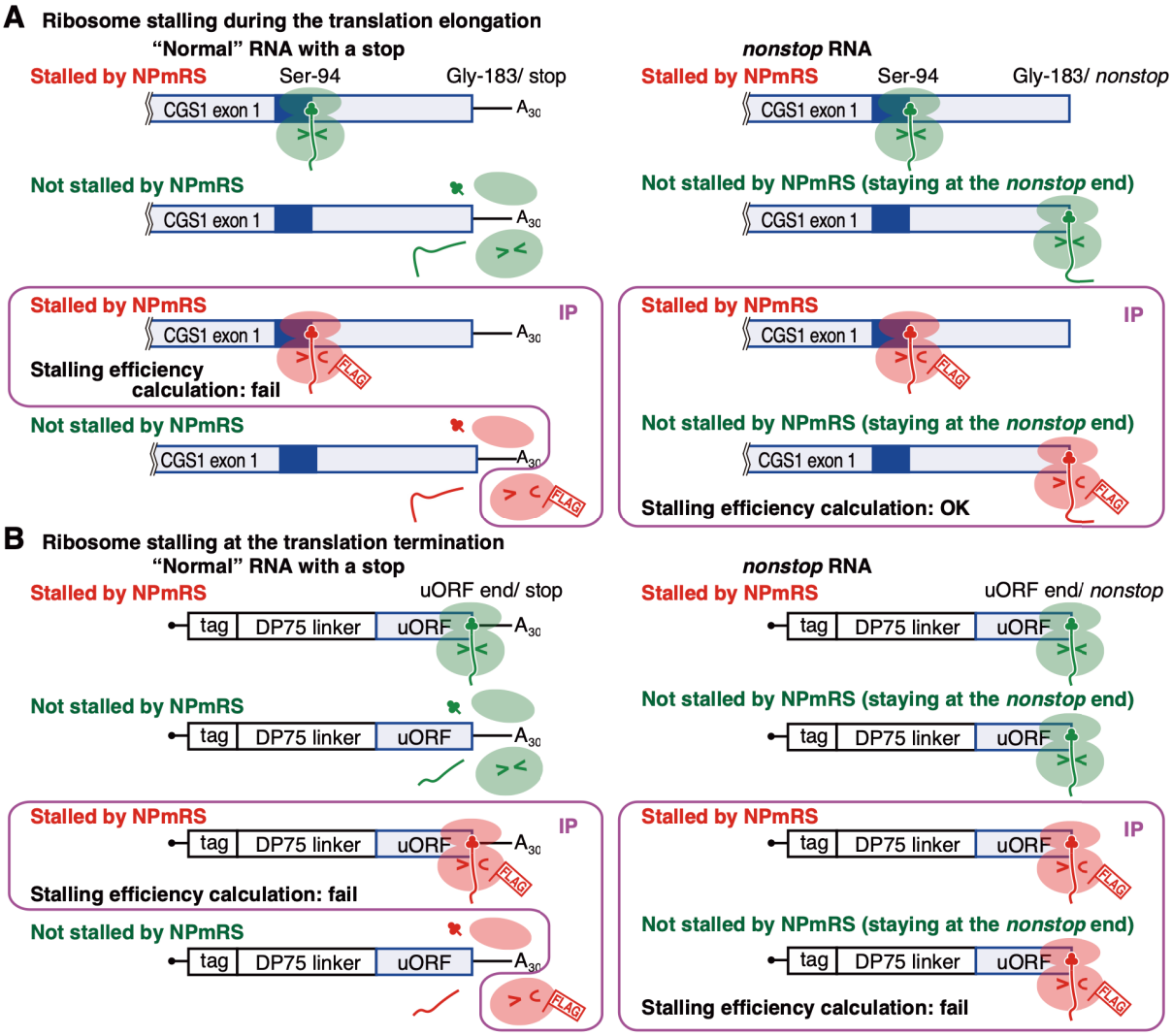

Supplementary Figure S9. Affinity purification strategy of the stalled ribosomes. The green ribosomes represent wild-type ribosomes, and the red ribosomes represent FLAG-tagged mutant ribosomes. tRNAs are represented by clovers. To calculate the stalling efficiency of FLAG-tagged mutant ribosomes alone, peptidyl-tRNAs from both stalled and non-stalled mutant ribosomes have to be purified. (**A**) Affinity purification of ribosomes stalled during the translation elongation by IP. The MTO1 region (21) is indicated by a filled blue box. (*Left*) On a "normal" RNA with a stop codon, those ribosomes that did not stall by NPmRS will translate to the stop codon and dissociate into large and small subunits and peptidyl-tRNA are hydrolyzed to tRNA and peptides. Therefore, those ribosomes that did not stall by NPmRS cannot be affinity-purified. (*Right*) On a *nonstop* RNA, those ribosomes that did not stall by NPmRS will translate to the *nonstop* RNA end and will be staying there. Therefore, both of them can be affinity-purified and stalling efficiency can be calculated. (**B**) Affinity purification of ribosomes stalled at the translation termination by IP. (*Left*) On a "normal" RNA with a stop codon, those ribosomes that did not stall by NPmRS will translate to the stop codon and dissociate into large and small subunits and peptidyl-tRNA are hydrolyzed to tRNA and peptides. Therefore, those ribosomes that did not stall by NPmRS cannot be affinity-purified. (*Right*) On a *nonstop* RNA, those ribosomes that did not stall by NPmRS will be staying at the *nonstop* RNA end. Therefore, both stalled and non-stalled ribosomes can be affinity-purified. However, stalling efficiency cannot be calculated, because these ribosomes bear the same peptidyl-tRNA species.

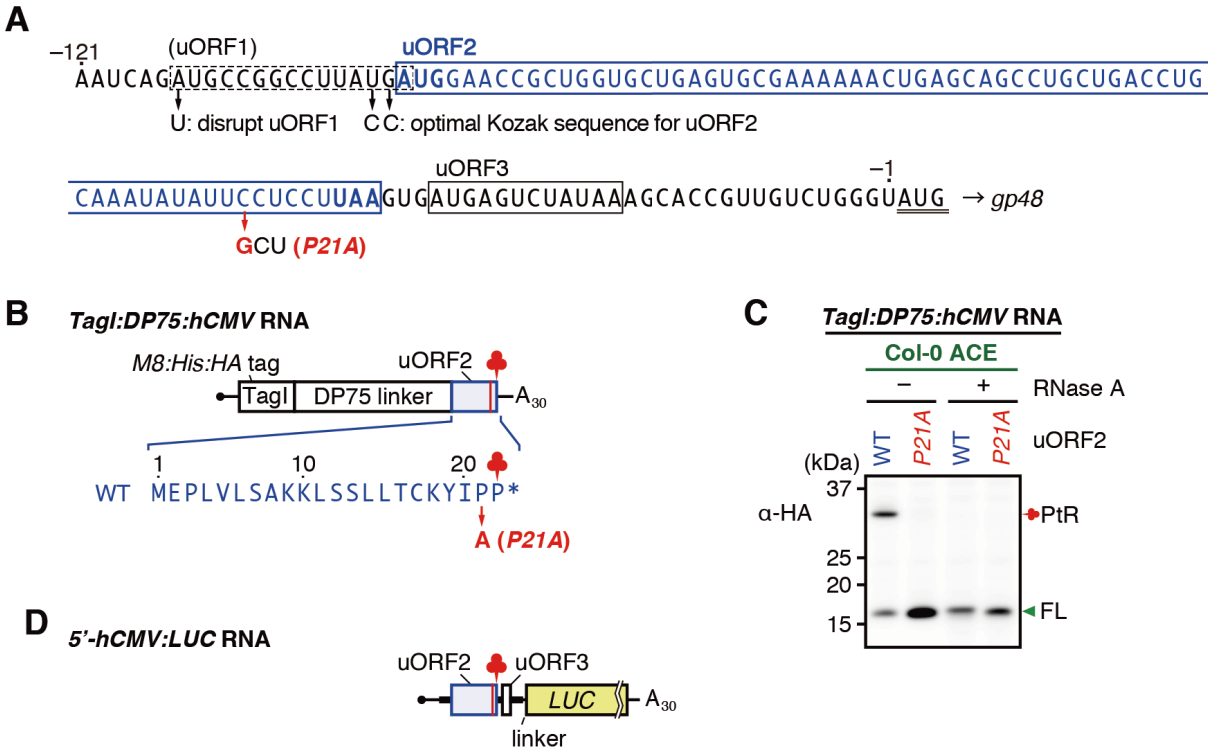

Supplementary Figure S10. The hCMV system in Col-0 ACE. (**A**) 5′-UTR sequence of hCMV *gp48* (46). uORFs are boxed and the start codon of *gp48* is double-underlined. uORF2 is the functional uORF for NPmRS. uORF1 (dashed box) was disrupted and the Kozak sequence for uORF2 was optimized in previous studies (27,29,46,65), and the same sequence was used in the present study. The substituted nucleotide in Pro-21 to alanine mutation (P21A) in uORF2, which abolishes the NPmRS (65), is indicated. (**B**) Schematic representation of *TagI:DP75:hCMV* RNA for stalling assay (Figure 5B). The uORF2 was joined in-frame to the *M8:His:HA* tags (*TagI*) and DP75 linker. The amino acid sequences of the *gp48* uORF2 and *P21A* mutation are shown. Ribosome stalls autonomously at the stop codon of uORF2 (red clover). (**C**) *TagI:DP75:hCMV*(*WT*) and *TagI:DP75:hCMV*(*P21A*) RNAs were translated in Col-0 ACE for 30 min. Translation products were separated by SDS-PAGE and analyzed by immunoblotting using anti-HA antibody. For RNase + lanes, samples were treated with RNase A before separation by SDS-PAGE. The positions of the 15-kDa full-length product (FL) and the 35-kDa peptidyl-tRNA (PtR) are indicated. A representative result of duplicate experiments is shown. (**D**) Schematic representation of *5′-hCMV:LUC* RNA used for reporter assay (Figure 7A). The 5′-UTR sequence (−1 to −121 nt) in (A) was joined to the *LUC* reporter gene through a linker sequence, AAGCUUUCC.

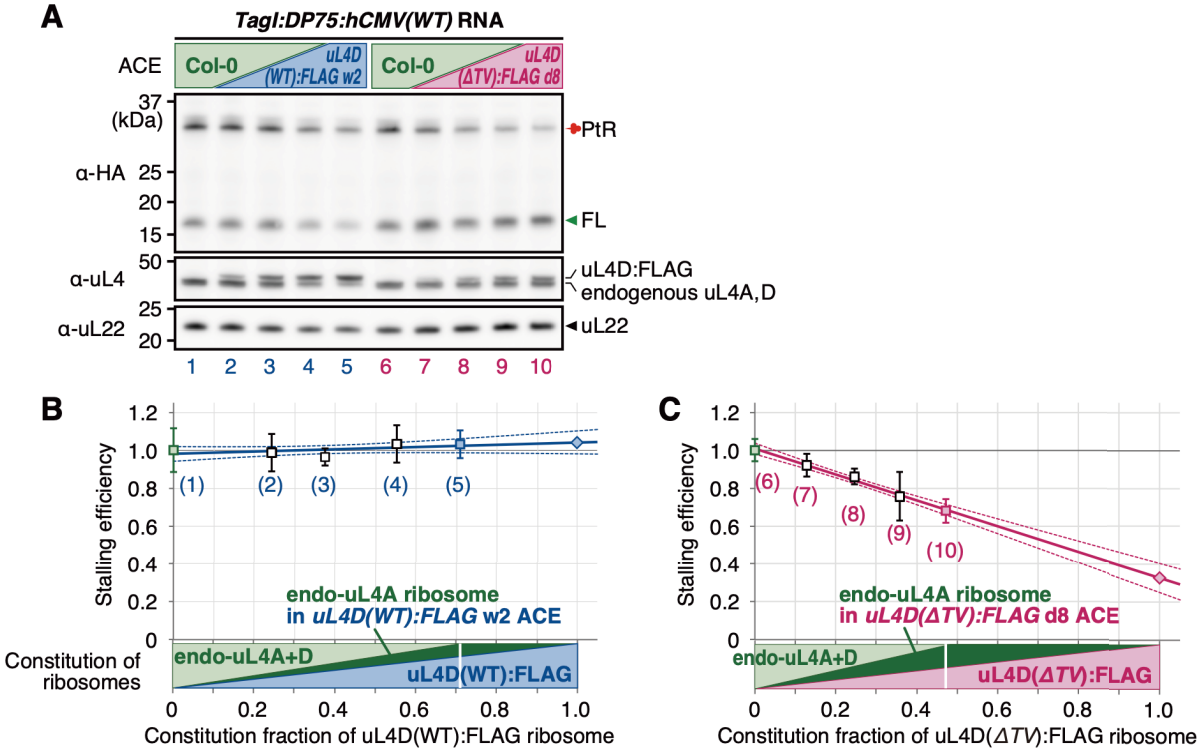

Supplementary Figure S11. Deduction of the stalling efficiencies by the mutant ribosomes alone by linear regression. (**A**) Col-0 ACE and uL4D(WT):FLAG line w2 ACE were mixed at 1:0, 3:1, 1:1, 1:3, and 0:1 volume ratios (lanes 1 to 5, respectively), or Col-0 ACE and uL4D(*ΔTV*):FLAG line d8 ACE were mixed at 1:0. 3:1, 1:1, 1:3, and 0:1 volume ratios (lanes 6 to 10, respectively). These mixtures were used to translate *Tag1:DP75:hCMV*(*WT*) RNA (Supplementary Figure S10B). Translation products were separated by SDS-PAGE and analyzed by immunoblotting using anti-HA antibody. Immunoblots with anti-uL4 and anti-uL22 are also shown. Positions of the full-length product (FL), peptidyl-tRNA (PtR), 48-kDa FLAG-tagged uL4Ds (uL4D:FLAG), endogenous uL4A and uL4D (uL4A, D), and 19-kDa uL22 are marked. The experiments were carried out in one of the batches of ACE preparations for each of the Col-0 and mutant lines, and a representative result of triplicate experiments is shown. (**B**) Linear regression (solid blue line) of stalling efficiency vs construction fraction of uL4D(WT):FLAG ribosome. Raw stalling efficiencies obtained from lanes 1–5 of (A) were plotted against the constitution fractions of the uL4D(WT):FLAG ribosome of each of the ACE mixtures (means ± SD, $n = 3$). The constitution fraction was determined based on the intensities of the upper and lower bands of the immunoblot with anti-uL4 antibody (Figure 4C and D). The numbers in parentheses below the data refer to the lane numbers in (A). The blue diamond indicates the estimated stalling efficiency by the uL4D(WT):FLAG ribosome alone. The dashed blue curves represent the upper and lower limits of the mean prediction 95% confidence interval. (**C**) Linear regression (solid magenta line) of stalling efficiency vs construction fraction of uL4D(*ΔTV*):FLAG ribosome. Raw stalling efficiencies obtained from lanes 6–10 of (A) were plotted against the constitution fractions of the uL4D(*ΔTV*):FLAG ribosome of each of the ACE mixtures (means ± SD, $n = 3$). The constitution fraction was determined as in (B). The numbers in parentheses below the data refer to the lane numbers in (A). The magenta diamond indicates the estimated stalling efficiency by the uL4D(*ΔTV*):FLAG ribosome alone. The dashed magenta curves represent the upper and lower limits of the mean prediction 95% confidence interval. In (B) and (C), calculated constitution fractions of endogenous uL4A- and D-containing ribosomes in Col-0 ACE (light green), endogenous uL4A-containing ribosomes in the mutant ACE (dark green), and FLAG-tagged mutant uL4D-containing ribosomes (light blue or light magenta) are shown below the graph. Note that to the right of the vertical white lines are extrapolated values. The linear regression and mean prediction 95% confidence interval were calculated using Mathematica software (Wolfram Research, Champaign, IL, USA).

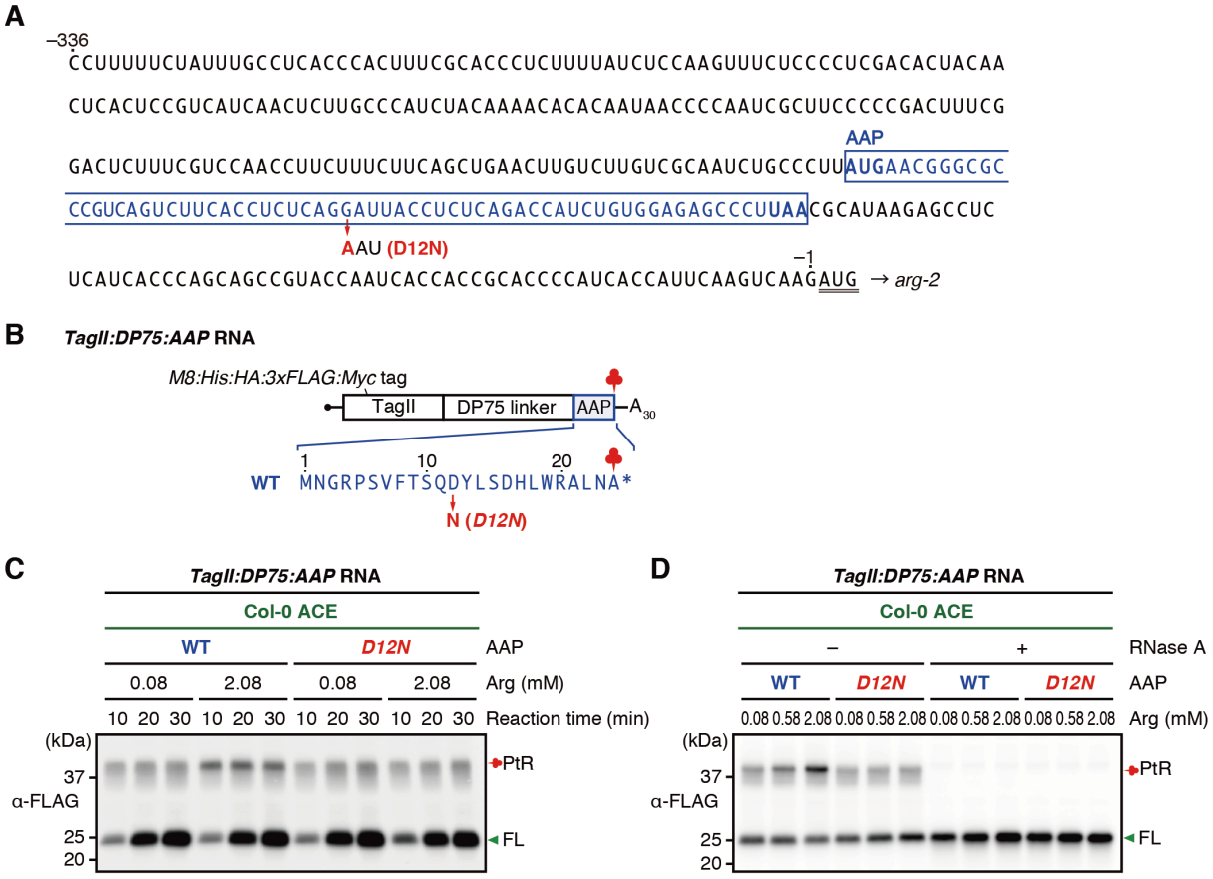

Supplementary Figure S12. The AAP system in Col-0 ACE. (**A**) The 5′-UTR sequence of *N. crassa arg-2* (24). uORF (AAP) is boxed and the start codon of *arg-2* is double-underlined. The nucleotide substituted in Asp-12 to asparagine (*D12N*) mutation is indicated. *D12N* mutation abolishes the L-arginine-dependent NPmRS of AAP (24). (**B**) Schematic representation of *TagII:DP75:AAP* RNA used for stalling assay (Figure 5C). The AAP sequence was joined in-frame to the *M8:His:HA:3xFLAG:Myc* tags (*TagII*) and DP75 linker. The amino acid sequences of AAP and *D12N* mutation are shown. L-Arginine-dependent NPmRS occurs at the stop codon (red clover). (**C**) *TagII:DP75:AAP*(*WT*) and *TagII:DP75:AAP*(*D12N*) RNAs were translated in Col-0 ACE at 0.08 or 2.08 mM L-arginine (Arg). Translation products were withdrawn at the indicated time points and analyzed by immunoblotting using anti-FLAG antibody. The positions of the 37-kDa peptidyl-tRNA (PtR) and 20-kDa full-length product (FL) are indicated. A representative result of duplicate experiments is shown. (**D**) *TagII:DP75:AAP*(*WT*) and *TagII:DP75:AAP*(*D12N*) RNAs were translated in Col-0 ACE for 10 min at different Arg concentrations. Translation products were analyzed as in (C). For RNase + lanes, samples were treated with RNase A before separation by SDS-PAGE. A representative result of duplicate experiments is shown.

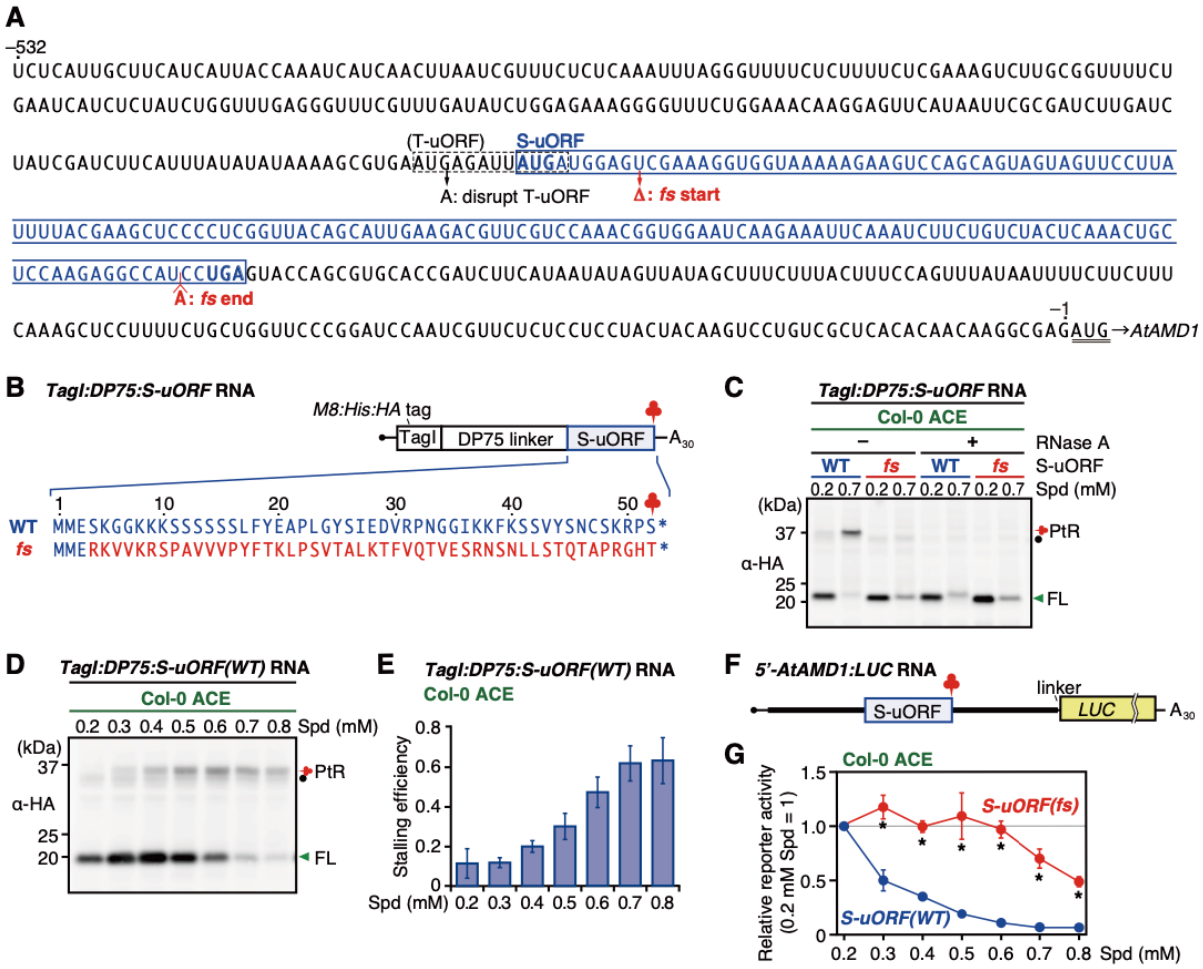

Supplementary Figure S13. The AtAMD1 system in Col-0 ACE. (**A**) The 5′-UTR sequence of *AtAMD1* (31). The 5′-UTR sequence of *AtAMD1* has two uORFs, T-uORF and S-uORF (standing for Tiny-uORF and Small-uORF, respectively) (30). The S-uORF is boxed and the start codon of *AtAMD1* is double-underlined. The T-uORF was disrupted as in a previous study (31) and is marked with a dashed box. The nucleotides that are deleted and inserted to generate the frame-shift mutant are indicated. (**B**) Schematic representation of *TagI:DP75:S-uORF* RNA used for stalling assay (Figure 5D). The S-uORF sequence was joined in-frame to the *M8:His:HA* tags (*TagI*) and DP75 linker. The amino acid sequences of *AtAMD1* S-uORF and frame-shift (*fs*) mutation are shown. Polyamine-dependent NPmRS occurs at the stop codon of S-uORF (red clover) (31). (**C**) *TagI:DP75:S-uORF*(*WT*) and *TagI:DP75:S-uORF*(*fs*) RNAs were translated in Col-0 ACE for 30 min at 0.2 or 0.7 mM spermidine (Spd). Translation products were separated by SDS-PAGE and analyzed by immunoblotting using anti-HA antibody. For RNase + lanes, samples were treated with RNase A before separation by SDS-PAGE. The positions of the 37-kDa peptidyl-tRNA (PtR) and 18-kDa full-length product (FL) are indicated. A black dot indicates a nonspecific signal. A representative result of duplicate experiments is shown. (**D**) *TagI:DP75:S-uORF*(*WT*) RNA was translated in ACE at various Spd concentrations. Translation products were analyzed as in (C). A representative result of triplicate experiments is shown. (**E**) The immunoblot signals in (D) were quantified and the raw stalling efficiencies were calculated. Means ± SD of three independent experiments are shown. (**F**) Schematic representation of *5′-AtAMD1:LUC* RNA used for reporter assay (Figure 7B). The 5′-UTR sequence (−1 to −532) in (A) was joined to the *LUC* reporter gene through a linker, CC. (**G**) *5′-AtAMD1:LUC*(*WT*) and *5′-AtAMD1:LUC*(*fs*) RNAs were translated in Col-0 ACE for 120 min at various Spd concentrations. LUC activity was normalized with control RLUC activity from co-translated *RLUC* RNA, and the reporter activity relative to that at 0.2 mM Spd was calculated. Means ± SD of three independent experiments are shown. Asterisks indicate significant differences at each Spd concentration ($p < 0.05$, Welch's *t*-test).

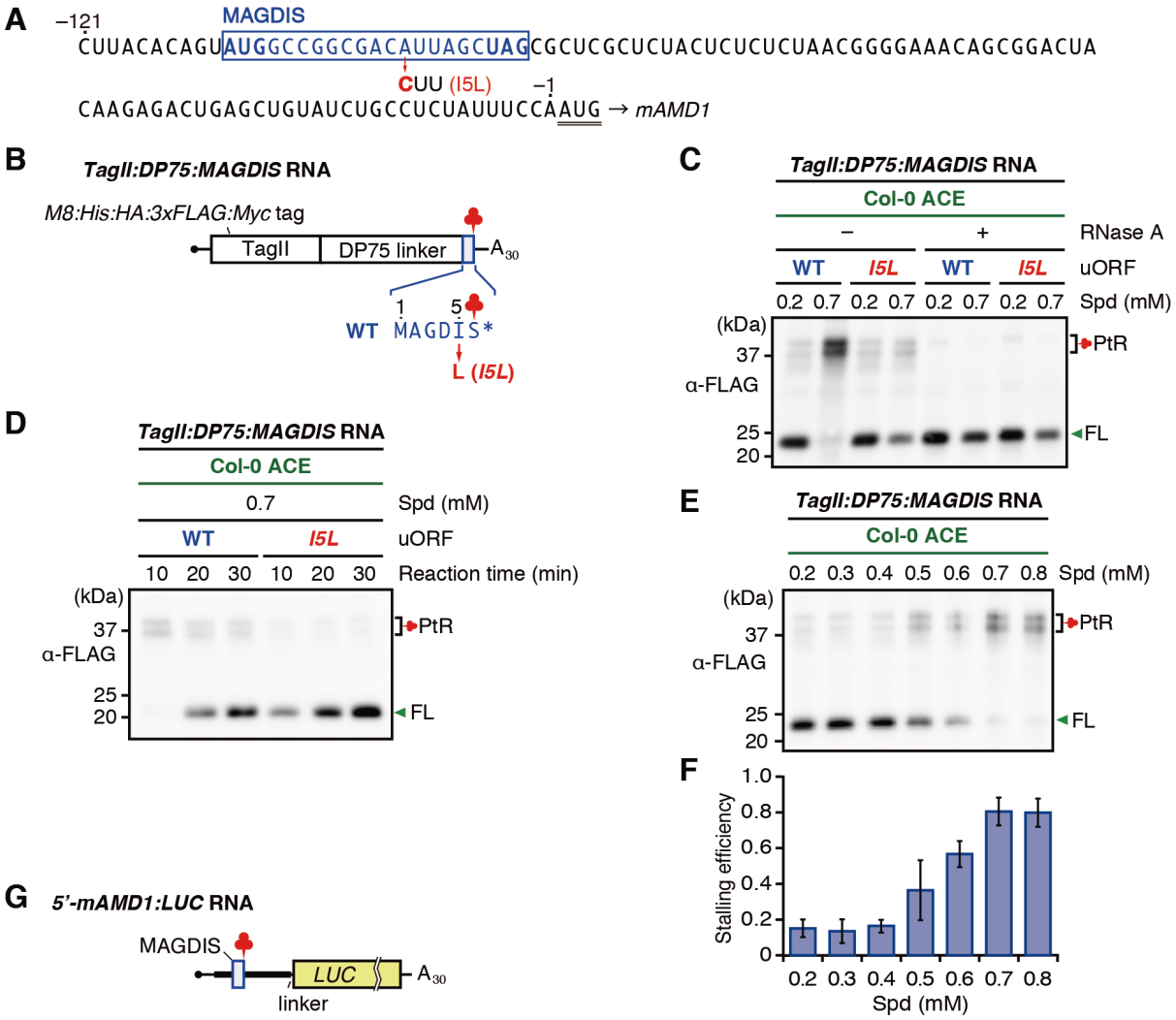

Supplementary Figure S14. The MAGDIS system in Col-0 ACE. (**A**) The 5′-UTR sequence of *mAMD1* (47,69). uORF is boxed and the start codon of *mAMD1* is double underlined. The nucleotide substituted in *I5L* mutant, which abolishes the stalling (32), is indicated. (**B**) Schematic representation of *TagII:DP75:MAGDIS* RNA used for stalling assay (Figure 5E). The uORF sequence was joined in-frame to the *M8:His:HA:3xFLAG:Myc* tags (*TagII*) and DP75 linker. The amino acid sequences of WT and *I5L* mutation are shown. (**C**) *TagII:DP75:MAGDIS*(*WT*) and *TagII:DP75:MAGDIS*(*I5L*) RNAs were translated in Col-0 ACE for 10 min at 0.2 or 0.7 mM spermidine (Spd). Translation products were analyzed by immunoblot analysis using anti-FLAG antibody. The positions of the 20-kDa full-length product (FL), and the 38-kDa peptidyl-tRNAs (PtR) are indicated. For RNase + lanes, samples were treated with RNase A before separation by SDS-PAGE. (**D**) *TagII:DP75:MAGDIS*(*WT*) RNA and *TagII:DP75:MAGDIS*(*I5L*) RNA were translated in Col-0 ACE at 0.7 mM Spd. Translation products were withdrawn at the indicated time points and analyzed by immunoblot analysis as in (C). (**E**) *TagII:DP75:MAGDIS*(*WT*) RNA was translated in ACE at various Spd concentrations. Translation products were analyzed as in (C). (**F**) The immunoblot signals in (E) were quantified and the raw stalling efficiencies were calculated. Means ± SD of three independent experiments are shown. (**G**) Schematic representation of *5′-mAMD1:LUC* RNA used for reporter assay (Figure 7C). The 5′-UTR (−1 to −121) sequence in (A) was joined to the *LUC* reporter gene through a linker, CC.

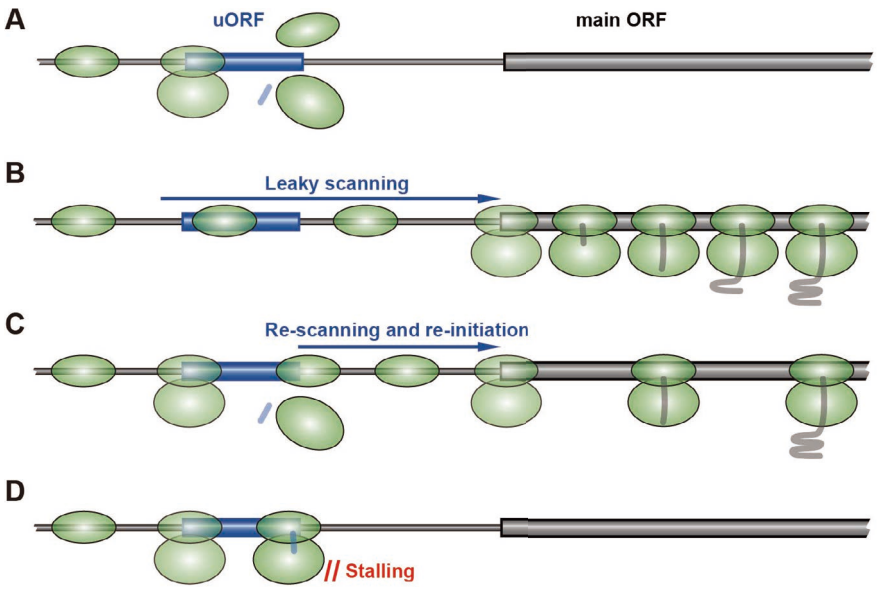

Supplementary Figure S15. Downregulation of the main ORF expression by uORF. The translation status of the uORF regulates translation of the downstream ORF, including the main ORF (59,70,71). The presence of uORF is not exceptional because 40%–50% of mRNAs in mammals and 30%–40% of mRNAs in higher plants have one or more of them (71,72). Many of the uORFs are actually translated, as evidenced by ribosome profiling analyses that showed the presence of 80S ribosomes on the uORFs (55,73). (**A**) Translation of a uORF generally downregulates the translation of the main ORF because those ribosomes that have translated the uORF will be dissociated from the mRNA (59). (**B**) The uORF may occasionally be overlooked and then translation starts at the start codon of the main ORF by a mechanism termed leaky scanning (74,75). The nucleotide sequence around the start codon, known as the Kozak sequence (70,76), of uORF plays a major role in determining the frequency of leaky scanning. (**C**) When a very short uORF is translated, the ribosome may not be fully dissociated at the termination codon and the small subunit may remain on the mRNA. The small subunit re-scans for the downstream start codon and reinitiates translation there (71,73,77). (**D**) If the ribosome stalls on the uORF, translation of the downstream ORF is severely inhibited by blocking the succeeding ribosomes (59). The ribosome stalling on uORF can occur either during translation elongation or at translation termination, while most of the known stalling events in eukaryotes occur at the termination.

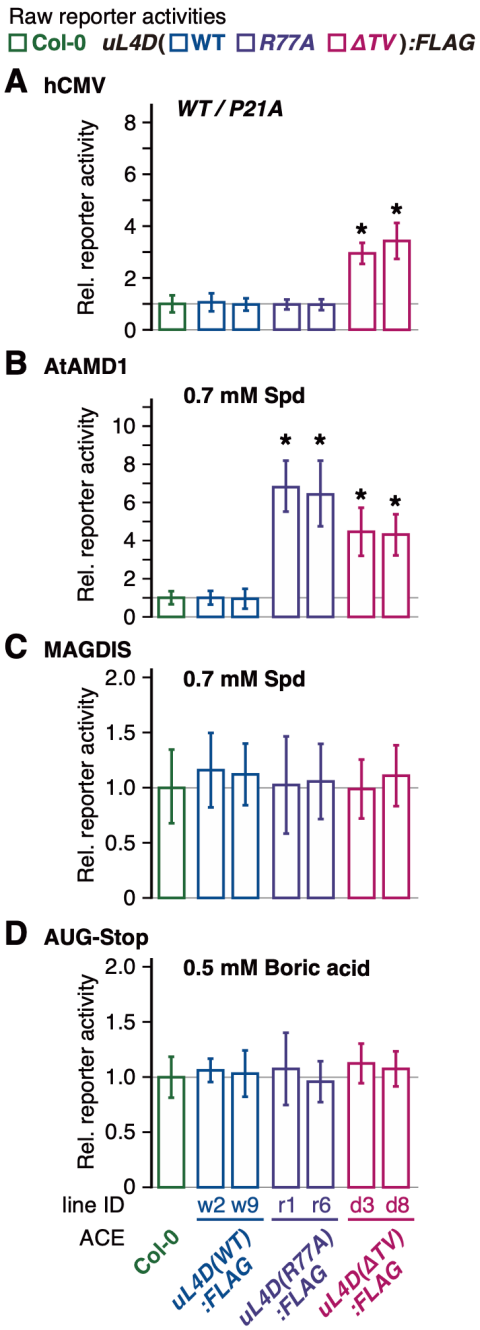

Supplementary Figure S16. Raw reporter activities. (**A**–**D**) The raw reporter activities corresponding to Figure 7A–D, respectively, are shown. Asterisks indicate significant differences compared with Col-0 ACE ($q < 0.05$ by Welch's *t*-test with FDR correction).

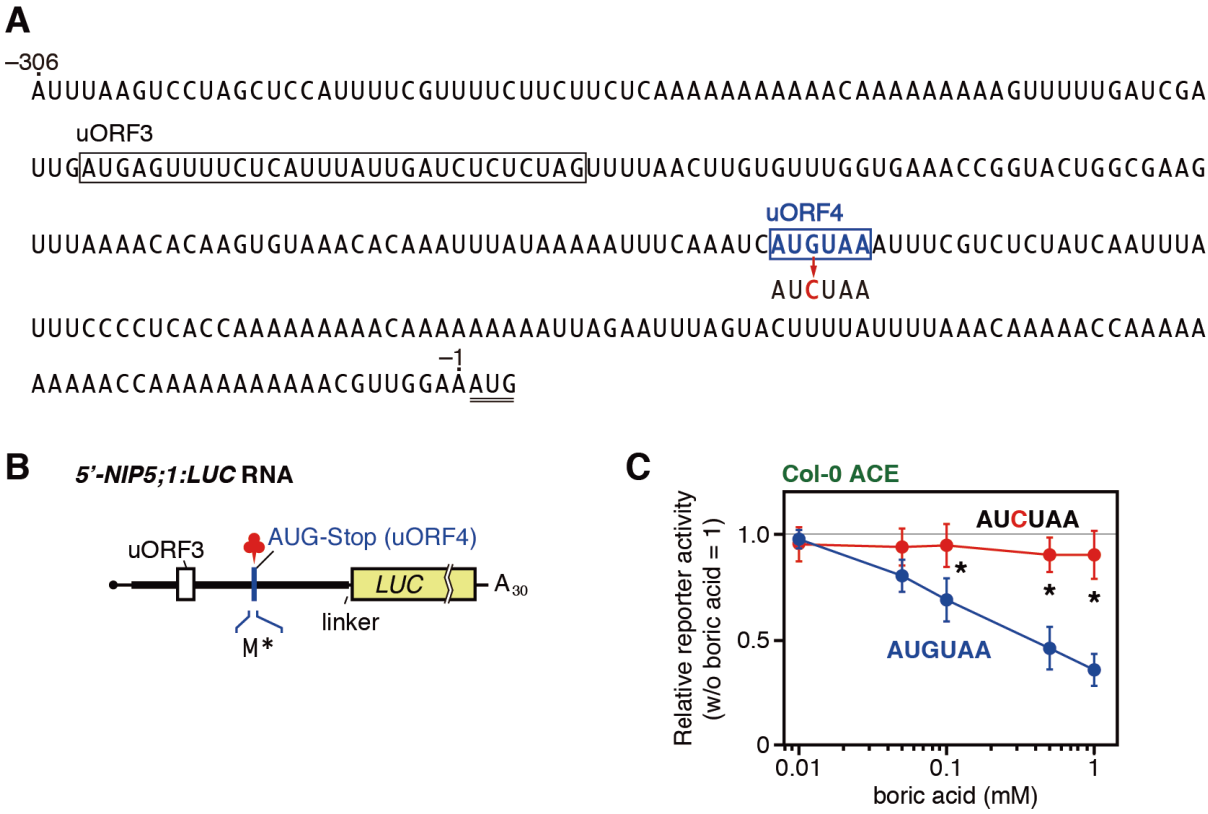

Supplementary Figure S17. The AUG-Stop system in Col-0 ACE. (**A**) The 306-nt 5′-UTR sequence of *AtNIP5;1* (34). The uORFs are boxed and the start codon of *AtNIP5;1* is double-underlined. The nucleotide substituted in *AUCUAA* mutant is indicated. (**B**) Schematic representation of *5′-NIP5;1:LUC* RNA used for reporter assay (Figure 7D). The 306-nt 5′-UTR sequence was joined to the *LUC* reporter gene through a linker, CC. (**C**) *5′-NIP5;1:LUC*(*AUGUAA*) and *5′-NIP5;1:LUC*(*AUCUAA*) RNAs were translated in Col-0 ACE for 120 min at various boric acid concentrations. LUC activity was normalized with control RLUC activity from co-translated *RLUC* RNA, and the reporter activity relative to that without boric acid was calculated. Asterisks indicate significant differences at each boric acid concentration ($p < 0.05$, Welch's *t*-test).

Supplementary Table S1. Plasmids used in this study and primers used to construct plasmids.

Name	Construct[a]	Source	Primers[b]	
			Forward	Reverse
Plasmids used for construction of transgenic Arabidopsis				
pYTJ10	*uL4D::uL4D(WT):FLAG*	this study	uL4Df	uL4Dr
pYTJ1	*uL4D::uL4D(R77A):FLAG*	this study	R77Af	R77Ar
pYTJ7	*uL4D::uL4D(ΔTV):FLAG*	this study	dTVf	dTVr
pYTJ4	*uL4D::uL4D(Δloop):FLAG*	this study	dLoopf	dLoopr
Plasmids used for stalling assay				
pST00	*SP6::M8:His:HA:DP75*	this study	DP75f	DP75r
pST55	*SP6::M8:His:HA:DP75:AAP(WT)*	this study	AAPf	AAPr
pST56	*SP6::M8:His:HA:DP75:AAP(D12N)*	this study	D12Nf	AAPr
pST57	*SP6::M8:His:HA:DP75:hCMV(WT)*	this study	hCMVf	hCMVr
pST58	*SP6::M8:His:HA:DP75:hCMV(P21A)*	this study	hCMVf	P21Ar
pST76	*SP6::M8:His:HA:DP75:S-uORF(WT)*	this study	SAMDC1f	SAMDC1r
pST77	*SP6::M8:His:HA:DP75:S-uORF(fs)*	this study	SAMDC1fsf	SAMDC1fsr
pST116	*SP6::M8:His:HA:DP75:MAGDIS(WT)*	this study	DP75f	MAGDISr
pST117	*SP6::M8:His:HA:DP75:MAGDIS(I5L)*	this study	DP75f	I5Lr
pTI5	*SP6::M8:His:HA:3xFLAG:Myc:DP75:AAP(WT)*	this study	3xFLAGf	3xFLAGr
pTI6	*SP6::M8:His:HA:3xFLAG:Myc:DP75:AAP(D12N)*	this study	3xFLAGf	3xFLAGr
pNU14	*SP6::GST:S-uORF(WT):RLUC*	Ref. 31		
pNU15	*SP6::GST:S-uORF(fs):RLUC*	Ref. 31		
pYF2	*SP6::GST:CGS1(WT)*	Ref. 68		
pYF3	*SP6::GST:CGS1(mto1-1)*	Ref. 68		
pYK00	*SP6::M8:CGS1(WT)*	Ref. 18		
pYY105	*T7::His:HA:DP75:uORF2(WT)*	Ref. 43		
Plasmids used for reporter assay				
pST118	*SP6::mAMD1 5′-UTR(WT):LUC*	this study	MAGDIS(WT)f	MAGDIS(WT)r
pST119	*SP6::mAMD1 5′-UTR(I5L):LUC*	this study	MAGDIS(I5L)f	MAGDIS(WT)r
pST120	*SP6::AtAMD1 5′-UTR(WT):LUC*	this study	SAMDC1f2	SAMDC1r2
pST121	*SP6::AtAMD1 5′-UTR(fs):LUC*	this study	SAMDC1f2	SAMDC1r2
pST122	*SP6::gp48 5′-UTR(WT):LUC*	this study	hCMVf2	hCMVr2
pST123	*SP6::gp48 5′-UTR(P21A):LUC*	this study	hCMVf2	P21Ar2
pMI21	*SP6::CGS1:LUC(WT)*	Ref. 22		
pMI27	*SP6::RLUC*	Ref. 22		
pMT131	*SP6::AtNIP5;1 5′-UTR(WT):LUC*	Ref. 34		
pMT132	*SP6::AtNIP5;1 5′-UTR(ATCTAA):LUC*	Ref. 34		
pSY209	*SP6::S-uORF(WT):RLUC*	Ref. 31		
pSY214	*SP6::S-uORF(fs):RLUC*	Ref. 31		

[a]Double colons indicate fusion of promoter sequence and an ORF, and single colons indicate an in-frame translational fusion (*i.e.*, *Promoter::ORF:ORF: ...*).

[b]Primers used for construction. Sequences of the primers are listed in Supplementary Table S2.

Supplementary Table S2. Primers used in this study.

Name	Sequence (5' to 3')	Source
Plasmid construction [a]		
uL4Df	CACCGGAGTATTGTTGCCCTTTGTGAA	this study
uL4Dr	CTGACTAGCGCCAAGCCACTT	this study
R77Af	ACCGGAGCTGCCGTGTCACGTA	this study
R77Ar	GTGACACGGCAGCTCCGGTT	this study
dTVf	TGGGGAGGAAGAGCCTCACGTATCCCTCGTGTTC	this study
dTVr	GTGAGGCTCTTCCTCCCCAGGACTCGGC	this study
dLoopf	TCCGCCGGAAGAGCCGGTGGTGGAACTCACCG	this study
dLoopr	ACCGGCTCTTCCGGCGGAGGTTTGGTGA	this study
uL4Flankf	CACCGGAGTATTGTTGCCCTTTGTGAA	this study
uL4Flankr	CTGACTAGCGCCAAGCCACTT	this study
DP75f	GATTCTAGACATCATCATCATCATCATTACCC	this study
DP75r	CATGGATCCGGCCATTCTGATATCCATTTCAATTTTATTGTCACT	this study
AAPf	CATGATATCATGAACGGTCGCCCGTCAGTCTTCACTAGTCAGGATTACCTCTCAGACC ATC	this study
AAPr	CTAGGATCCGAGAGGCTCTCACGCGTTAAGGGCTCTCCACAGATGGTCTGAGAGG	this study
D12Nf	CATGATATCATGAACGGTCGCCCGTCAGTCTTCACTAGTCAGAATTACCTCTCAGACC ATC	this study
hCMVf	CATGATATCATGGAACCGCTGGTGCTGAGTGCGAAAAAACTGAGCAGCCTGCTGAC	this study
hCMVr	CTAGGATCCTCGAGTGCTTTAAGGAGGAATATATTTGCAGGTCAGCAGGC	this study
P21Ar	CTAGGATCCTCGAGTGCTTTAAGGAGCAATATATTTGCAGGTCAGCAGGC	this study
hCMVf2	GATTCTAGAAATCAGTTGCCGGCCTTACCATGGAACCGCTGGTGCTGAGTGCGAAAAA ACTGAGCAGCCTGCTGACCTGC	this study
hCMVr2	CATAAGCTTACCCAGACAACGGTGCTTTATAGACTCATCACTTAAGGAGGAATATATT TGCAGGTCAGCAGGC	this study
P21Ar2	CATAAGCTTACCCAGACAACGGTGCTTTATAGACTCATCACTTAAGGAGCAATATATT TGCAGGTCAGCAGGC	this study
SAMDC1f	CATGATATCATGATGGAGTCGAAAGGTG	this study
SAMDC1r	CTAGGATCCTCAGGATGGCCTCTTGGA	this study
SAMDC1fsf	CATGATATCATGATGGAGCGAAAGGTG	this study
SAMDC1fsr	CTAGGATCCTCAGGTATGGCCTCTTGGA	this study
SAMDC1f2	GATTCTAGATCTCATTGCTTCATCATTACCA	this study
SAMDC1r2	CATCCATGGCTCGCCTTGTTGTGTGAG	this study
MAGDISr	CATGGATCCCTAGCTAATGTCGCCGGCCATGATATCCATTTC	this study
I5Lr	CATGGATCCCTAGCTAAGGTCGCCGGCCATGATATCCATTTC	this study
MAGDIS(WT)f	GATTCTAGACTTACACAGTATGGCCGGCGACATTAGCTAGCGCTCGCTCTACTCTCTC TAACGGGGAAACAG	this study
MAGDIS(I5L)r	GATTCTAGACTTACACAGTATGGCCGGCGACCTTAGCTAGCGCTCGCTCTACTCTCTC TAACGGGGAAACAG	this study
MAGDIS(WT)r	CATCCATGGTGGAAATAGAGGCAGATACAGCTCAGTCTCTTGTAGTCCGCTGTTTCCC CGTTAG	this study
Myc:DP75f	TCAGAGGAGGACCTGGAAGGTGGCGAAGAAGAAGTTGAG	this study
HAMycr	GATCAGCTTCTGCTCAGCGTAATCTGGAACATCGTATGGG	this study
Mycf	GAGCAGAAGCTGATCTCAGAGGAG	this study
HAr	AGCGTAATCTGGAACATCGTATGGG	this study
3xFLAGf	GTTCCAGATTACGCTGACTACAAAGACCATGACGGTGATTATAAAGATCATGACATCG ACTACAAAGACG	this study
3xFLAGr	GATCAGCTTCTGCTCCTTGTCGTCATCGTCTTTGTAGTCGATGTCATGATC	this study
Generating DNA templates for in vitro transcription		
SP65'fp	CATCAGAGCAGATTGTACTG	Ref. 18
G183r	ACCGGCATGAACAGT	this study
poly(A)r	ACGAGCCGGAAGCATAAAG	this study
Quantitative RT-PCR		
RT-uL4Af	AAGAAGAAGGGGTATGTGCT	this study
RT-uL4Ar	CACCGAGCCATTTGGTGAAGT	this study
RT-uL4Df	GGGTTAAGGCTAAGAAGGAG	this study

RT-uL4Dr	TCGGTGTAGTCACTGTCTGA	this study
RT-FLAGf	ACAGTGACTACACCGAGTTC	this study
RT-FLAGr	TCATCGTCATCCTTGTAGCT	this study
UBQ5f	GTGGTGCTAAGAAGAGGAAGA	this study
UBQ5r	TCAAGCTTCAACTCCTTCTTT	this study

[a]Restriction sites used for cloning the PCR-amplified fragments are underlined.

SUPPLEMENTARY REFERENCES

65. Geballe, A.P., Spaete, R.R. and Mocarski, E.S. (1986) A *cis*-acting element within the 5' leader of a cytomegalovirus β transcript determines kinetic class. *Cell*, **46**, 865–872.

66. International Wheat Genome Sequencing Consortium (2018) Shifting the limits in wheat research and breeding using a fully annotated reference genome. *Science*, **361**, eaar7191.

67. Murota, K., Hagiwara-Komoda, Y., Komoda, K., Onouchi, H., Ishikawa, M. and Naito, S. (2012) Corrigendum: Arabidopsis cell-free extract, ACE, a new in vitro translation system derived from Arabidopsis callus cultures. *Plant Cell Physiol*., **53**, 602.

68. Haraguchi, Y., Kadokura, Y., Nakamoto, M., Onouchi, H. and Naito, S. (2008) Ribosome stacking defines *CGS1* mRNA degradation sites during nascent peptide-mediated translation arrest. *Plant Cell Physiol*., **49**, 314–323.

69. Ruan, H., Shantz, L.M., Pegg, A.E. and Morris, D.R. (1996) The upstream open reading frame of the mRNA encoding *S*-adenosylmethionine decarboxylase is a polyamine-responsive translational control element. *J. Biol. Chem*., **47**, 29576–29582.

70. Kozak, M. (1986) Point mutations define a sequence flanking the AUG initiator codon that modulates translation by eukaryotic ribosomes. *Cell*, **44**, 283–292.

71. von Arnim, A.G., Jia, Q. and Vaughn, J.N. (2014) Regulation of plant translation by upstream open reading frames. *Plant Sci*., **214**, 1–12.

72. Crowe, M.L., Wang, X.Q. and Rothnagel, J.A. (2006) Evidence for conservation and selection of upstream open reading frames suggests probable encoding of bioactive peptides. *BMC Genomics*, **7**, 16.

73. Wethmar, K. (2014) The regulatory potential of upstream open reading frames in eukaryotic gene expression. *Wiley Interdiscip. Rev. RNA*, **5**, 765–778.

74. Kozak, M. (1999) Initiation of translation in prokaryotes and eukaryotes. *Gene*, **234**, 187–208.

75. Kozak, M. (2002) Pushing the limits of the scanning mechanism of initiation of translation. *Gene*, **299**, 1–34.

76. Joshi, C.O., Zhou, H., Huang, X. and Chiang, V.L. (1997) Context sequences of translation initiation codon in plants. *Plant Mol. Biol*., **35**, 993–1001.

77. Kozak, M. (1987) Effects of intercistronic length on the efficiency of reinitiation by eukaryotic ribosomes. *Mol. Cell. Biol*., **7**, 3438–3445.